Hindawi
Shock and Vibration
Volume 2023, Article ID 6951186, 17 pages
https://doi.org/10.1155/2023/6951186

Research Article

Impact of Tuned Mass Dampers and Electromagnetic Tuned Mass Dampers on Geometrically Nonlinear Vibrations Reduction of Planar Cable Robots

Diego A. Zamora-Garcia, Alejandro C. Ramirez-Reivich, and Ma. Pilar Corona-Lira

National Autonomous University of Mexico, School of Engineering, Mexico City, Mexico

Correspondence should be addressed to Diego A. Zamora-Garcia; diego.zamora@ingenieria.unam.edu

Received 30 August 2022; Revised 14 January 2023; Accepted 22 February 2023; Published 23 March 2023

Academic Editor: Emiliano Mucchi

Vibration is one of the problems that limits the applications of cable driven parallel robots (CDPR). The problem is bigger in CDPR with planar configuration due to the presence of out-of-plane vibrations, which have a larger amplitude and settling time. Some authors have proposed solutions such as the increase in tension of the wires, increase in the end effector mass, or the use of active dampers. In this research, we investigated the performance of tuned mass dampers (TMD) and electromagnetic tuned mass dampers (ETMD) which are integrated in the end effector of a CDPR in a planar configuration with eight wires. The essential idea is to reduce the settling time of the end effector through free vibrations without the use of external energy. This research followed an analytical and experimental methodology with the following steps. Three mathematical models were formulated and analysed using numerical simulations. Then, a test bench to validate the analytical results was designed and built. The effectiveness of the dampers was evaluated by comparing the settling times of the following three cases: without damper, with TMD, and with ETMD. During the investigation, it was observed that the use of AMS can reduce the settling time using the appropriate parameters. The effectiveness of AEMS is highly dependent on frictions and can be effective in some scenarios. Reductions in settling time from marginal values to 95% can be obtained. This research implies a viable solution for the out-of-plane vibrations of planar CDPR.

1. Introduction

A cable driven parallel robot, referred to as CDPR, is a parallel robot that uses flexible cables instead of rigid links. The movement of the end effector in the workspace is achieved through the coordinated retraction and extension of the cables. Some of the first works were made in Japan by Higuchi et al. [1] with applications in the construction and maintenance of facades, then another work was published in the USA by Dagalakis et al. [2] with shipbuilding applications. Since then, research on this topic has been expanded and various practical applications have been proposed.

As a new technology, there are some issues that should be resolved before applying it in a broader way. There are problems in the formulation of workspaces, force distribution [3], inverse kinematics, and inverse dynamics. Another problem is the vibration. Due to the inherent flexibility of the cables, the problem of vibration arises. Some authors have explored the vibrations in cable robots [4–6].

To reduce the vibrations in cable robots, different solutions have been proposed. One of these solutions is the increase in cable tension. With more tension in cables there is a higher vibration frequency and a lower amplitude. Another solution is the increase of the mass of the end effector. With a greater mass, the final effector is less susceptible to external disturbances. Some other solutions include active systems to reduce vibration [7–11]. All these solutions solve the problem to some extent, but they have a general problem. In all the previous solutions, extra energy for the system was needed. One of the advantages of cable robots is that they use low energy and have little moving

mass. If we use the previous solutions, we could be eliminating these advantages.

Of all the possible types of vibrations in the CDPR, the out-of-plane vibrations are the most problematic. This is because they have the biggest vibratory amplitude and the largest settling time in the out-of-plane direction of the CDPR. These kind of vibrations are present in planar configurations, where one direction does not have a direct mechanical restriction. A design of this kind of CDPR can be seen in [12]. This kind of vibration and this configuration of a CDPR were the study cases in this research.

The out-of-plane vibrations in planar cable robot configurations need to be reduced. A solution could be a shock absorber or a damper. This damper must not be connected to the mechanical reference because the end effector of the CDPR moves throughout the workspace during its operation. One candidate is a tuned mass damper, or TMD. The linear TMD is a well-studied option to mitigate vibrations in structures; it just needs to be connected to the vibratory structure and not to the mechanical reference. It consists in attenuating the vibration of a structure by placing a second degree of freedom and tuning the mass, the spring, and in some cases the damper. The evolution of this technology can be seen in the work of Villaverde [13] in which it is shown in its beginnings, the work of Sadek et al. [14] and the article of Bekdas and Nigdeli [15] who implemented a new strategy of optimization. Theoretical research about the use of TMD in cable robots has been presented [16]. Research has been carried out on the use of geometric nonlinearities for use in TMD [17]. There is another option to reduce the vibrations with a damper that does not need to be in contact with a mechanical reference. The electromagnetic tuned mass damper, or ETMD. This is an innovation in the TMD technology and it consists of incorporating relative movement between a coil of cooper and a magnetic field. This is implemented between the first and second degrees of freedom. The research on this technology is more recent. Some significant works in ETMD are by Fleming and Moheimani [18] who created an active control, Tang and Zuo [19], and Zuo and Cui [20].

This paper investigates the performance of TMD and ETMD as potential solutions for the out-of-plane vibrations of planar CDPR. The focus of this study is the mitigation of the settling time of the vibration in the end effector of the cable robot. This vibration is studied when the robot is not executing a trajectory, that is, when the end effector is not moving through the workspace. In the case of TMD, the variables stiffness and mass of the damper are varied. In the case of ETMD, the variables electromechanical coupling coefficient and load resistance are varied.

The remainder of this paper is organized as follows: Section 2 describes the mathematics used to build three models: the vibration without damper, the vibration with TMD, and the vibration with ETMD. To achieve this, the equations that define the geometric nonlinearities of springs and dampers were deduced. These were used as building blocks. The experimental procedure that shows the construction of a test bench and the protocols for experimentation are presented in Section 3. Section 4 presents the analytical and experimental results of the research. Finally, the discussion and pertinent conclusions are provided in Section 5.

2. The Mathematical Model of the Dynamic System

This section shows the development of three mathematical models. These are the vibrations without TMD, the vibration with TMD, and the vibration with ETMD. According to the diagram in Figure 1, the CDPR workspace is the plane $x_f - y_f$ according to the framework h_f. The cables are connected at one end to the mechanical reference and at the other end to the end effector. The cables lie on the $x_f - y_f$ plane. The robot end effector and the magnetic field (permanent magnet) represent the first degree of freedom z_1 in the z_f direction. A coil of copper with its assembly elements represents the second degree of freedom z_2 in the z_f direction. The displacement of the end effector in the direction are the out-of-plane vibrations. It can be better seen in Figure 2 with a view from the $z_f - y_f$ plane. The first mathematical model was elaborated, taking into account the equivalent elasticity and viscosity of the cables. Then the dynamic elements of the TMD were incorporated to build the second model and finally the dynamic elements of the ETMD were incorporated to build the third model.

2.1. Geometrically Nonlinear Vibrations. The out-of-plane vibrations are described as the oscillations of the end effector of the cable robot in the z_f direction according to the framework h_f. In this research, the phenomenon was studied when the end effector is vibrating in the z_f direction but it is not moving in the workspace. The end effector is in the workspace centre, where the least stiffness in the z_f direction occurs. These vibrations could have different causes, like momentary external disturbances to misalignments in the mechanical assembly. In this work, the causes are not studied; the goal is to solve the vibration that already occurs.

The critical element of the cable robot that promotes the vibrations due to its inherent flexibility is the steel cable. As shown in Figure 2, when the out-of-plane vibrations occur, the cable experiences a change in their axial elongation and in its direction. This is described as geometrically nonlinear behaviour. The cables are modelled as a spring and damper in parallel with negligible mass; this is a Kelvin–Voight model. Other authors have modelled the cable in a similar way [21], and some experimental works about the axial viscoelasticity of a steel wire with this model have been published [22].

Figure 3 shows a diagram that represents the dynamics of a cable with geometrically nonlinear oscillations. The b_{cn} represents the viscous friction coefficient of the n-th cable and k_{cn} represents the spring constant of the n-th cable. These elements are linear in their axial direction. At the top, the cable is attached to a mechanical reference; at the bottom, it is attached to the A point, which travels in the positive and negative direction z_f according to the

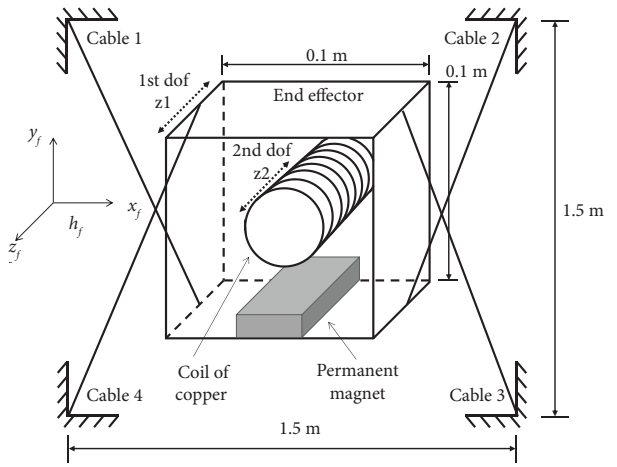

Figure 1: Diagram of the planar CDPR and the ETMD inside the end effector, elements that represent two degrees of freedom in the z_f direction.

established framework $h_?$. The cable length l_n is the instant length, and if the system is in oscillation, then the value of l_n is changing all the time. The original cable length l_{on} occurs when the cable is in its equilibrium position, which is vertical with the angle $\theta_?$ equal to zero. At this time, l_{on} is equal to l_n. It is important to mention that the cable, in its equilibrium state, should have a minimum tension of zero and a maximum that depends on the resistance of the cable and the mechanical structure.

The process for modelling spring and damper force in the z_f direction is described below. The forces through the cable at all moments due to the spring and the pretension, are defined by f_{cn}. This is the sum of the spring force f_{ckn}, and the pretension f_{ptn}, as shown in the following equation:

$$f_{cn} = f_{ckn} + f_{ptn}. \tag{1}$$

The force of interest in this application is the one that exerts the equivalent spring of the cable in the z_f direction, that is, the component of $f_{??}$ in the z_f direction. This force is called f_{kzn}. Its nomenclature means the force (f) of the spring (k) in the direction of (z) of the n-th wire (n). This can be achieved by multiplying equation (1) by sin (θ_n), and the result is shown in the following equation:

$$\begin{aligned} f_{kzn} &= f_{cn}\sin(\theta_n) \\ &= \left(f_{ckn} + f_{ptn}\right)\sin(\theta_n). \end{aligned} \tag{2}$$

The force due to the elongation of the spring f_{ckn} can be defined as a function of the original length l_{on} and the instant length l_n using Hooke's law, as shown in the following equation:

$$f_{ckn} = k_{cn}(l_n - l_{\text{on}}). \tag{3}$$

The displacement in z_f, the original length l_{on}, and the Pythagorean theorem are used to get the instantaneous length of the cable. The instantaneous length l_n is defined as the hypotenuse, as stated in the following equation:

$$l_n = \sqrt{l_{on}{}^2 + z^2}. \tag{4}$$

The instantaneous length l_n can be substituted in equation (3) to make the equation a function of the variable to be measured and a known constant. This is shown in the following equation:

$$f_{ckn} = k_{cn}\left(\sqrt{l_{on}{}^2 + z^2} - l_{\text{on}}\right). \tag{5}$$

The force in z_f is exclusively due to the spring f_{kzn}, without considering the pretension that may exist in the cable, can be defined by known variables and constants by substituting equation (5) in equation (2). The result is the following equation:

$$f_{kzn} = k_{cn}\left(\sqrt{l_{on}{}^2 + z^2} - l_{\text{on}}\right)\sin(\theta_n). \tag{6}$$

It is possible to incorporate the pretension f_{ptn} of the cable. The following equation shows this:

$$f_{kzn} = \left(k_{cn}\left(\sqrt{l_{on}{}^2 + z^2} - l_{\text{on}}\right) + f_{ptn}\right)\sin(\theta_n). \tag{7}$$

The angles θ_n can be represented by known variables in the system, these are the displacement in z and the original length l_{on}. The Pythagorean theorem is used with the opposite side OS and the hypotenuse H. It is shown in the following equation:

$$\begin{aligned} \sin(\theta_n) &= \frac{OS}{H} \\ &= \frac{z}{\sqrt{l_{on}{}^2 + z^2}}. \end{aligned} \tag{8}$$

Substituting equation (8) in equation (7), the expression that defines the force of the cable in the z_f direction due to spring elongations and pretension is obtained, as shown in the following equation:

$$f_{kzn} = \frac{z\left(f_{ptn} - k_{cn}\left(l_{\text{on}} - \sqrt{l_{\text{on}}^2 + z^2}\right)\right)}{\sqrt{l_{\text{on}}^2 + z^2}}. \tag{9}$$

In the case of geometrically nonlinear damping, some authors have proposed some theoretical models that can be found in [23–25]. The general expression for the force generated by a linear viscous damper f_{bn} as a function of its velocity is the well-known equation shown in the following equation:

$$f_{bn} = b_{cn}\frac{\mathrm{d}z}{\mathrm{d}t}. \tag{10}$$

The term b_{cn} is the coefficient of viscous friction and Z is the position coordinate. The component of this force in the z_f direction is found using the sine of the angle θ_n and is called f_{bzn}. Its nomenclature means the force (f), due to the viscosity (b) in the direction of (z) of the n-th wire (n). The equation is as follows:

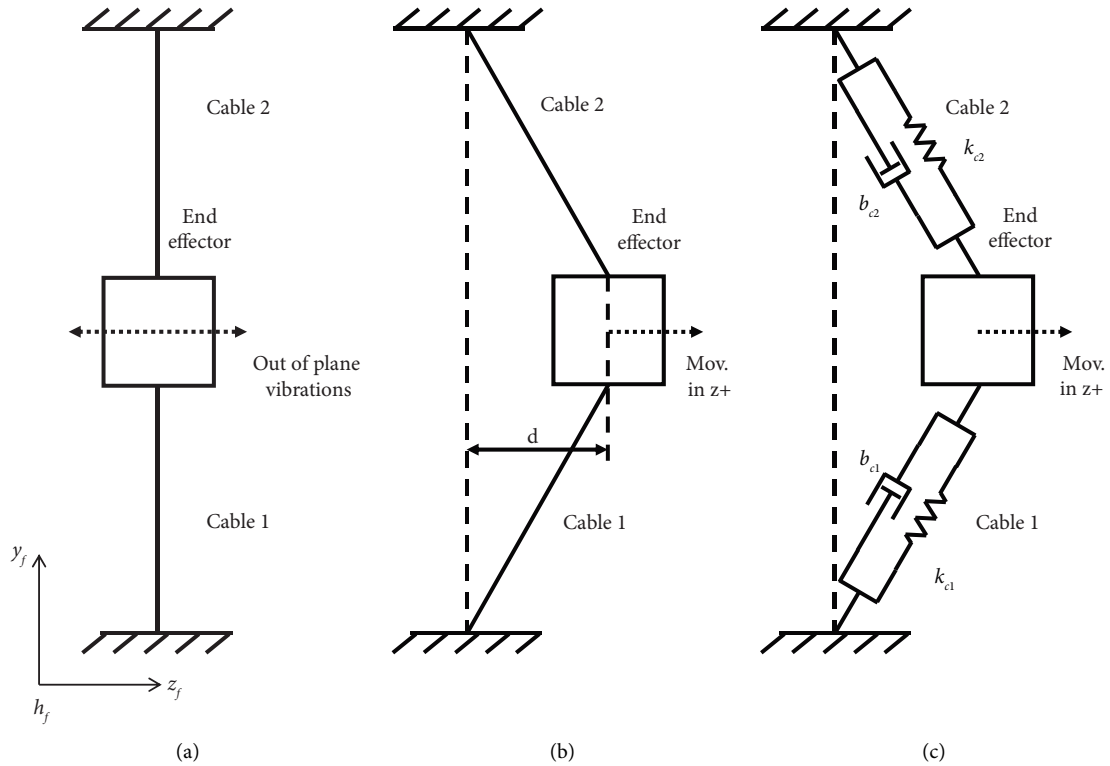

Figure 2: Representation of the out-of-plane vibrations. (a) End effector in its equilibrium position, (b) end effector out of its equilibrium position, and (c) cables with their equivalent viscoelastic model.

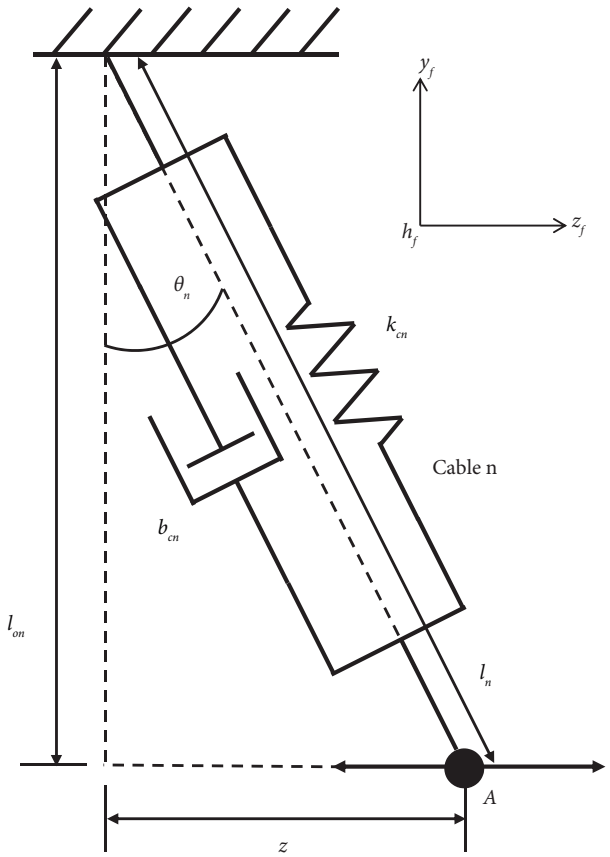

Figure 3: Diagram of the variables involved in the out-of-plane vibrations.

$$f_{bzn} = f_{cbn}\sin(\theta_n) = \left(b_{cn}\frac{dz}{dt}\right)\sin(\theta_n). \tag{11}$$

The angle θ_n can be presented by known variables in the system. This is the same procedure that was performed with the springs to eliminate the angle from the equation. This is shown in the following equation:

$$\sin(\theta_n) = \frac{OS}{H} = \frac{z}{\sqrt{l_{on}^2 + z^2}}. \tag{12}$$

By making the viscous damping coefficient considering the geometric properties of the damper at any position, equation (11) becomes the following equation:

$$f_{bn} = b_{cn}\frac{dz}{dt} = b_{cn}\left(\frac{z}{\sqrt{l_{on}^2 + z^2}}\right)\frac{dz}{dt}. \tag{13}$$

Finally, after making the corresponding substitutions, the component of the damper force in the z_f direction is expressed as a function of the position and the velocity of the z_1 coordinate, as shown in the following equation:

$$f_{bzn} = b_{cn}\left(\frac{z^2}{l_{\text{on}}^2 + z^2}\right)\frac{dz}{dt}. \tag{14}$$

The force of the spring in the z_f direction represented by equation (9) and the force of the damper in the z_f direction represented by equation (14) are the constitutive blocks to build the three dynamic models. Dynamic diagrams of the three models are shown in Figure 4. For reasons of space and cleanliness in the diagram the eight cables are represented by just two cables (Cable 1 and Cable 2). Parameters implied in each model can be appreciated.

2.2. Vibrations without Damper-First Model. The dynamic diagram of the first model is shown in Figure 4(a). There is a frame of reference called h_f. The mass of the end effector m_e, oscillates in the z_f direction and represents the first degree of freedom z_1. The cables have original lengths l_{o1} and l_{o2}, and instantaneous lengths l_1 and l_2 that change all the time during the vibration and are related to the angles θ_1 and θ_2. The cables have an equivalent internal elasticity and viscosity named k_{c1}, b_{c1}, k_{c2}, yb_{c2}. The gravity is acting in the negative direction y_f, and the force that exerts in the end effector is presented in the diagrams as W_e. The friction of the end effector with the air is presented in the diagrams as F_f.

For this first model of one degree of freedom there is one differential equation with some terms associated to the geometric nonlinearities of the cables, this is shown in the following equation:

$$m_e\frac{\mathrm{d}^2 z_1}{\mathrm{d}t^2} + b_f\frac{\mathrm{d}z_1}{\mathrm{d}t} + F_{kzA} + F_{kzB} + F_{bz} = 0. \tag{15}$$

The term F_{kzA} represents the sum of forces in the z_f direction due to the equivalent springs of the upper cables including the tension T_w, due to the weight of the end effector. There are four of these forces associated to the four upper cables. The term F_{kzB} represents the sum of forces in the z_f direction due to the equivalent springs of the lower cables (cables that do not carry the weight of the end effector). There are four of these forces associated to the four lower cables. The term F_{bz} represents the sum of forces of in the z_f direction due to the equivalent dampers in all the eights cables. There are eight of these forces associated to the eight cables. This is shown in equations (16)–(21).

$$F_{kzA} = \sum_{n=1}^{4} F_{kznA}, \tag{16}$$

$$F_{kznA} = \frac{z_1\left(\left(f_{ptn} + T_w\right) - k_{cn}\left(l_{\text{on}} - \sqrt{l_{\text{on}}^2 + z_1^2}\right)\right)}{\sqrt{l_{\text{on}}^2 + z_1^2}}, \tag{17}$$

$$F_{kzB} = \sum_{n=1}^{4} F_{kznB}, \tag{18}$$

$$F_{kznB} = \frac{z_1\left(f_{ptn} - k_{cn}\left(l_{\text{on}} - \sqrt{l_{\text{on}}^2 + z_1^2}\right)\right)}{\sqrt{l_{\text{on}}^2 + z_1^2}}, \tag{19}$$

$$F_{bz} = \sum_{n=1}^{8} F_{bzn}, \tag{20}$$

$$F_{bzn} = b_{cn}\left(\frac{z_1^2}{l_{\text{on}}^2 + z_1^2}\right)\frac{\mathrm{d}z_1}{\mathrm{d}t}. \tag{21}$$

2.3. Vibrations with TMD-Second Model. The vibration of the end effector with the TMD implemented is the second model. This is shown in Figure 4(b)). There are new elements added to the model. There is a mas of the damper m_a which represents the second degree of freedom z_2. Between the end effector m_e and the mass of the damper m_a there is an elastic element k_a, a viscous friction b_a,and a dry friction μ.

For this model there is a set of two differential equations related to the two degrees of freedom. These are the equations (22) and (23).

$$m_e\frac{\mathrm{d}^2 z_1}{\mathrm{d}t^2} + F_{kzA} + F_{kzB} + F_{bz} + F_a + F_\mu + F_{ka} + F_{ba} = 0, \tag{22}$$

$$m_a\frac{\mathrm{d}^2 z_2}{\mathrm{d}t^2} + F_{ka} + F_{ba} + F_\mu = 0. \tag{23}$$

The terms F_{kzA}, F_{kzB}, and F_{bz} are the same as in model one. The term F_μ represents the force in the z_f direction between the first and the second degree of freedom due to the dry friction. This term involves the dry friction coefficient μ, the relative velocity of the masses, and the gravity. This is shown in the following equation:

$$F_\mu = (m_a \mathrm{g}\,\mu)\mathrm{sign}\left(\frac{\mathrm{d}z_1}{\mathrm{d}t} - \frac{\mathrm{d}z_2}{\mathrm{d}t}\right). \tag{24}$$

The terms $F_{ka} + F_{ba}$ are related to the linear elements of elasticity and viscosity in the damper. The term F_f represents the viscous friction of the first degree of freedom with the air. Putting together all the terms in the original equations, the full-dynamic model for the AMS on the out-of-plane vibrations is obtained, as shown in equations (25) and (26).

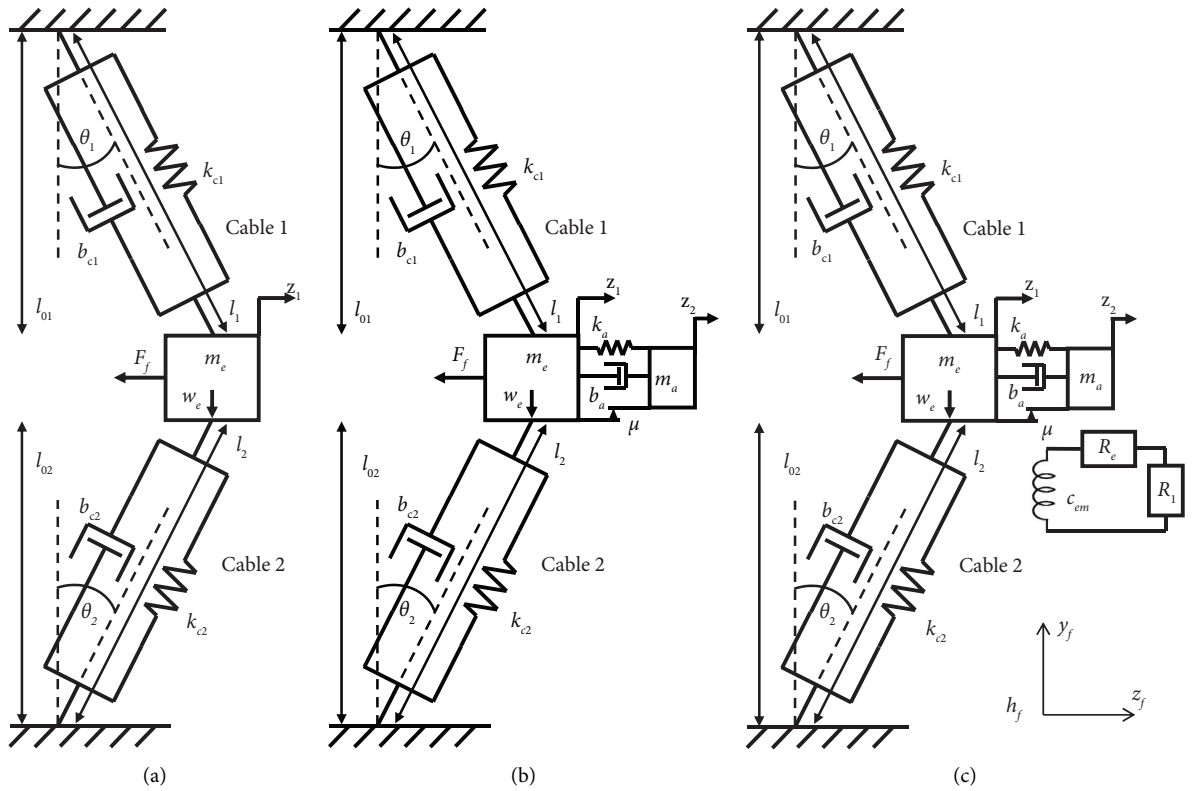

Figure 4: Dynamic diagrams of the three mathematical models. (a) Vibration without damper, (b) vibration with TMD, and (c) vibration with ETMD.

$$m_e\frac{d^2z_1}{dt^2}+b_f\frac{dz_1}{dt}+b_a\left(\frac{dz_1}{dt}-\frac{dz_2}{dt}\right)+(m_a g\mu)\text{sign}\left(\frac{dz_1}{dt}-\frac{dz_2}{dt}\right)+k_a(z_1-z_2)+F_{kzA}+F_{kzB}+F_{bz}=0, \tag{25}$$

$$m_a\frac{d^2z_2}{dt^2}+b_a\left(\frac{dz_2}{dt}-\frac{dz_1}{dt}\right)+(m_a g\mu)\text{sign}\left(\frac{dz_2}{dt}-\frac{dz_1}{dt}\right)+k_a(z_2-z_1)=0. \tag{26}$$

2.4. Vibrations with ETMD-Third Model. The dynamic diagram of the third model is shown in Figure 4(c)). The same frame of reference h_f is used. There are three new parameters in this model. The electro motive force is represented by the electromechanical coupling coefficient C_{em}. The electric resistance of the cooper coil is represented by R_e and the electric resistance of the load by R_l. In practice load resistor is the element that harvest energy.

The set of two differential equations of this third model is shown in equations (27) and (28).

$$m_e\frac{d^2z_1}{dt^2}+F_{kzA}+F_{kzB}+F_{bz}+F_a+F_\mu+F_{ka}+F_{ba}+F_{em}=0, \tag{27}$$

$$m_a\frac{d^2z_2}{dt^2}+F_{ka}+F_{ba}+F_\mu+F_{em}=0. \tag{28}$$

In the case of the AEMS implemented in the out-of-plane vibrations there is a magnetic field in the first degree of freedom and a coil of conductive material in the second degree of freedom. Therefore, an electromotive force is generated. The force reflected into the mechanical domain F_e. Considering Lorentz equation and velocity–voltage relationship, the term F_e can be written as a function of the velocity vel, as shown in the following equation:

$$F_e=\frac{(Bl)^2}{R_e+R_l}*\text{vel}. \tag{29}$$

The product of the magnetic field and the length of the wire in the coil Bl can be replaced for known variables using the electromechanical coupling coefficient C_{em}. Assuming the coil is exposed to a field of constant flux density and the relative displacement is small it results in the following equation:

$$\begin{aligned}\frac{\text{vol}}{\text{vel}} &= \frac{F_e}{i} \\ &= Bl \\ &= C_{em},\end{aligned} \tag{30}$$

where F_e denotes the force acting on the coil carrying a current i, and C_{em} is the ideal electromechanical coupling coefficient. When the coil is used as a generator it relates the induced voltage (vol) to a displacement. The set of two differential equations that define the full-dynamic model of an ETMD implemented in the out of plane vibrations are shown in equations (31) and (32).

$$m_e\frac{d^2z_1}{dt^2}+\left(b_a+b_f\right)\frac{dz_1}{dt}-b_a\frac{dz_2}{dt}+k_az_1-k_az_2+F_{kzA}+F_{kzB}+F_{bz}+\frac{(C_{em})^2}{R_e+R_l}\left(\frac{dz_1}{dt}-\frac{dz_2}{dt}\right)+(m_a g\mu)\text{sign}\left(\frac{dz_1}{dt}-\frac{dz_2}{dt}\right)=0, \tag{31}$$

$$m_a\frac{d^2z_2}{dt^2}+b_a\frac{dz_2}{dt}-b_a\frac{dz_1}{dt}+k_az_2-k_az_1+\frac{(C_{em})^2}{R_e+R_l}\left(\frac{dz_2}{dt}-\frac{dz_1}{dt}\right)+(m_a g\mu)\text{sign}\left(\frac{dz_2}{dt}-\frac{dz_1}{dt}\right)=0. \tag{32}$$

3. Experimental Set up

A test bench was designed and built to experimentally validate the proposed models. The test bench consisted of three parts, the mechanic, the electronic instrumentation, and the software. The mechanical assembly consists of a main structure made of aluminium profile, the mechanic reference. The end effector or first degree of freedom is in the centre of the structure and in the workspace centre, clamped to the main structure through eight cables. Inside the end effector there is a coil of conductive wire, which represents the second degree of freedom. Two types of sensors were used, two position laser sensors to measure the position of each degree of freedom and four load cells to measure the tension in the cables. This information is collected in an industrial computer and displayed in a human machine interface (HMI). A block diagram of the experimental setup is shown in Figure 5.

The displacement of the two degrees of freedom is in the z_f direction according to the reference frame h_f. The test bench has the capability to vary the following parameters, in the model without damper the parameters l_{on} and p_{tn}, in the model with TMD the parameters m_a and k_a, and in the model AEMS the parameters C_{em} and R_l, Figure 6 shows the test bench and the main parts that constitute it.

3.1. Mechanical Construction. The test bench consists of a main structure made of aluminium profile. Square workspace configurations with different dimensions and with the first degree of freedom in the centre can be mounted in the main structure. The end effector joins the main structure by four double cables from the corners of the square workspace. Therefore, the final effector is held by eight cables. Here, it is possible to change the first two variables of the experiment, the length l_{on} of the cables and the pretension level f_{ptn}. This can be done because there are mechanical elements that were especially designed for this purpose. For this research, the workspace is a square with 1.5 m per side.

The angular supports for load cells are high stiffness pieces made of steel located in each of the four corners of the workspace. These are the links between the aluminium main structure and the load cells. They can be moved and adjusted in the x_f direction and the C orientation. This is the rotation in the z_f direction. The length of the cables in the test bench can be varied moving one aluminium profile in the main structure and the position and orientation of the angular supports for load cells. Other pieces are the double cable tensioners. These are located at the ends of each of the four load cells. They are made of plastic and have two functions. The first function is to divide a single cable segment into two cable segments that hold the final effector in two points. The second function is to vary the tension of cable segments by means of an adjustment screw.

The end effector is in the workspace centre. This is composed for three subassemblies: the cube, the linear guide, and the magnetic field. The cube is a cubic structure 10 cm side made of aluminium profiles joined with plastic pieces; other elements are placed inside of this. The set linear guide is composed of two plastic supports and two stainless-steel linear guide. The set magnetic field is a plastic support with neodymium magnets whose distance with respect of the steel linear guide can be adjusted to vary the electromechanical coupling coefficient C_{em}. These three sets of elements make the first degree of freedom of the dynamical system. It is shown in Figure 7.

In the stainless-steel linear guides, there is a specially machined bushing in which a coil is mounted. Small metal bronze plates can be added or removed from the coil to vary the damper mass m_a. This is the second degree of freedom of the dynamical system. There are two springs that connect the first degree of freedom with the second degree of freedom. These springs can be replaced by different springs of the same length, but with different turns to vary the spring constant of the damper k_a. The bushing has viscous friction b_a and dry friction μ with the linear guides.

3.2. Electronic Instrumentation. The force in the cables was measured with four Omega brand load cells placed in each corner of the workspace. These have a force capacity of 30 N. The displacement of the two degrees of freedom was measured with two Omron brand laser sensors model XZ1-LD300A61. These have a resolution of 0.002 mm and

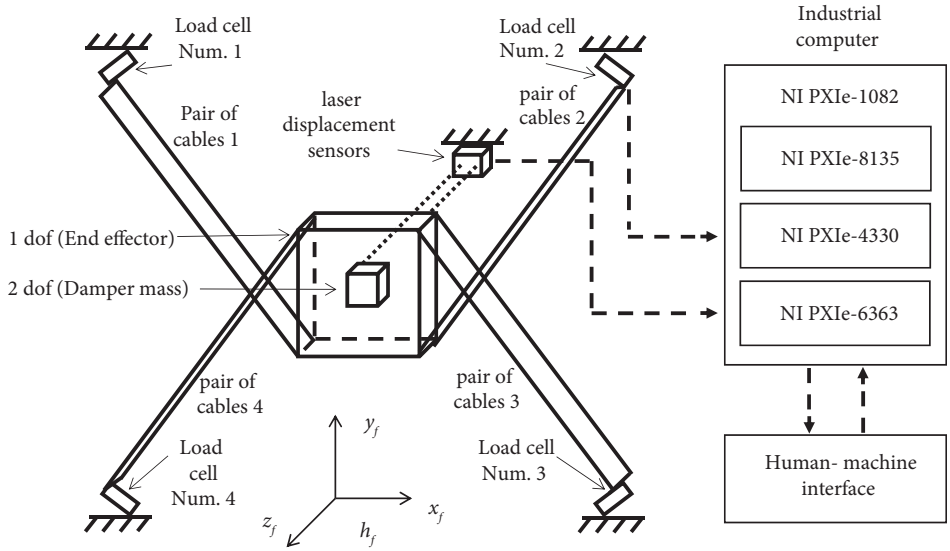

Figure 5: Block diagram of the experimental setup.

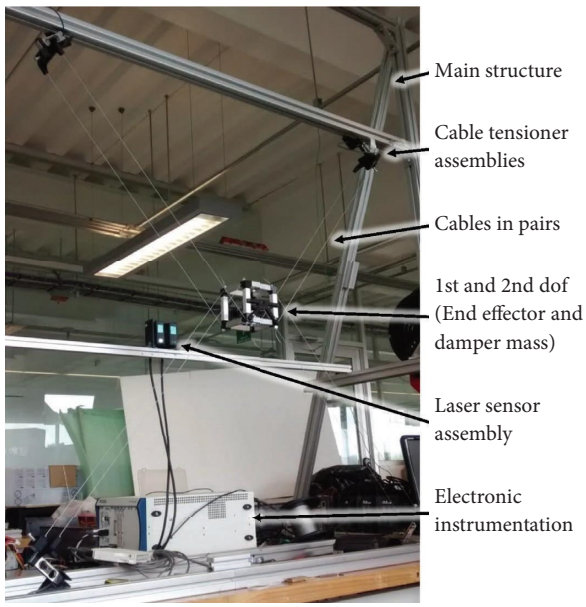

Figure 6: Photography of the experimental setup.

a maximum measuring range of 300 mm. To save the data, we used a National Instruments brand industrial computer model NI PXIe 1082, with a controller model NI PXIe 8135. In the chassis of the PXI, we used a module NI PXIe 4330 to measure load cells in a full-bridge configuration and a module NI PXIe 6363 to acquire the signals of the laser sensors. All the signals are acquiring at a frequency of 500 Hz.

3.3. Experimental Protocol. To evaluate the effectiveness of the AMS a numerical simulation was carried out using the mathematical model of equations (25) and (26). A three-dimensional surface was plotted, and the optimal parameters were found by exploring the plot. A theoretical settling time was found. These parameters were later set on the test bench, and experimental runs were carried out to compare with the theoretical results and validate the model. The parameters that were varied for the plotting were the mass damper m_a and spring constant of the damper k_a. In the case of frictions, these were kept at low levels as specified in Table 1. To evaluate the effectiveness of the AEMS, a similar procedure was performed using the mathematical model of equations (31) and (32), and an experimental validation procedure in the test bench. The varied parameters were the electromechanical coupling coefficient C_{em} and the load resistance R_l.

To perform the experimental test, after the parameters were adjusted in the test bench, the end effector was placed in the positive z_f direction at a point outside its equilibrium state. At that moment, the end effector is released and the

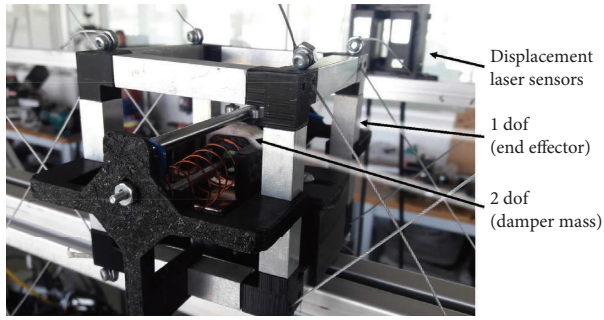

Figure 7: Photography of the first and second degrees of freedom.

Table 1: Dynamic system parameters.

Parameters	Description	Values	Units
First degree of freedom (end effector)			
m_e	End effector mass	0.5225	kg
b_f	Mass-air friction coefficient	0.0031	N/(m/s)
k_{c1}	Cable spring constant	25000	N/m
b_{c1}	Viscous coefficient of friction of the cable	90	N/(m/s)
T_w	Extra tension due to weight of 1st dof	3.4	N
l_{o1}	Original length of cables	1.06	M
f_{pt1}	Pretension in the cables	10	N
Second degree of freedom (damper mass)			
m_a	Damper mass	0.067	kg
k_a	Spring constant in damper	12	N/m
b_a	Viscous coefficient of friction of the damper	0.4	N/(m/s)
μ	Dry friction coefficient of the damper	0.1	Dimensionless
C_{em}	Electromechanical coupling coefficient	2.65	V/(m/s)
R_e	Coil electrical resistance	85.15	Ω
R_l	Electric load resistance	20	Ω

free vibration with the two degrees of freedom is recorded with the laser sensors. This procedure is performed for vibration without dampers, vibration with AMS, and vibration with AEMS. The final values of the dynamics system parameters are shown in Table 1.

4. Results

The research was conducted numerically in the first instance and later experimental validations were conducted. This section presents numerical and experimental results of the tree study cases, which are vibration without damper, vibration with TMD, and vibration with ETMD. The analytical data come from numerical simulations of the mathematical models using the Matlab® development environment. Point-by-point simulations were performed to build three-dimensional graphs and explore the optimal values, no other optimization method was used. The experimental results come from the designed test bench.

The geometrically nonlinear oscillations of springs and dampers have already been studied analytically in previous works [16]. It was found that in this oscillation there are zones of low stiffness and low energy dissipation centred on the equilibrium point of the dynamic system, and this is the cause of the large vibratory amplitudes and long settling times of the out of plane vibrations in planar CDPRs.

4.1. Vibration without Damper. The vibration without damper refers to the end effector-free vibration in the z_f direction represented by the equation (15). The two most important variables are the end effector mass m_e and the original cable lengths l_{on}, which have a direct effect on the settling time of the free vibration before an initial position condition of 30 mm in the z_f direction. The graph in Figure 8 shows a surface that defines the variation of end-effector settling time with respect to m_e and l_{on}.

Figure 9 shows simulated and real data of the free vibration with respect to time for three values of initial position (30 mm, 20 mm, and 10 mm). In the vibrational decay profile, the large vibratory amplitude and the long settling time is appreciated. The time on the horizontal axis of the graphs is 1200 s, which is 20 minutes. During

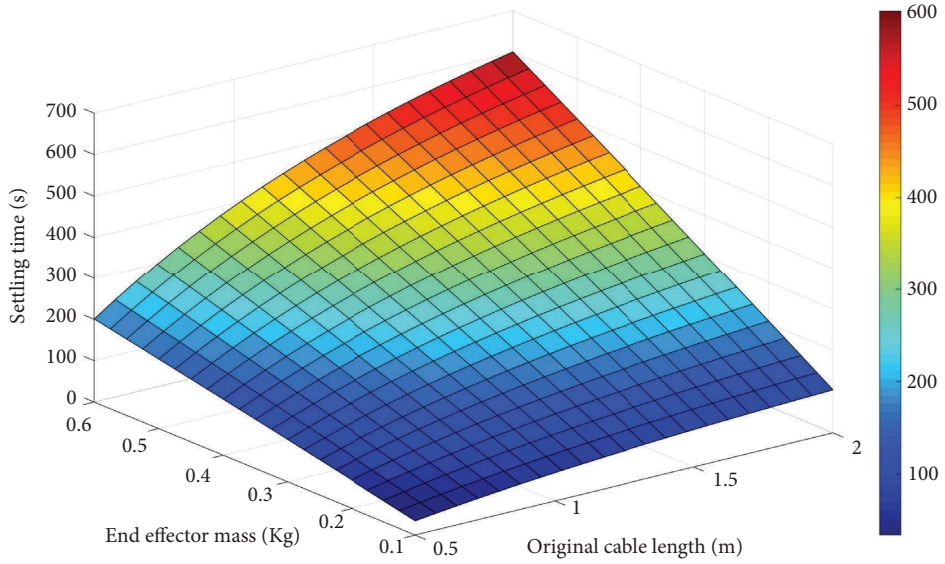

Figure 8: Surface of the settling time response to a change in parameters m_e and l_{on}. First model without damper.

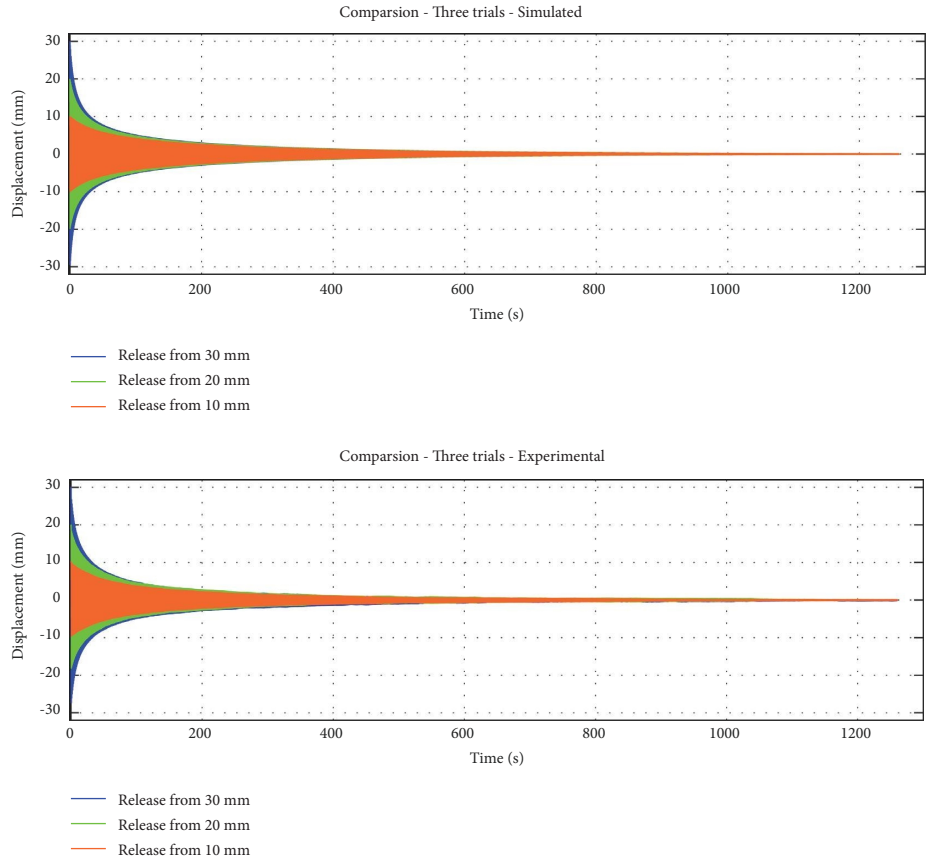

Figure 9: Simulated and real time responses of free vibrations for different initial conditions. First model without damper.

the first seconds of the oscillation a rapid reduction of the vibratory amplitude is indicated. The data show that lower values of the initial position imply a longer settling time. This contrasts with linear vibration in which a higher value in the initial position implies a longer settling time.

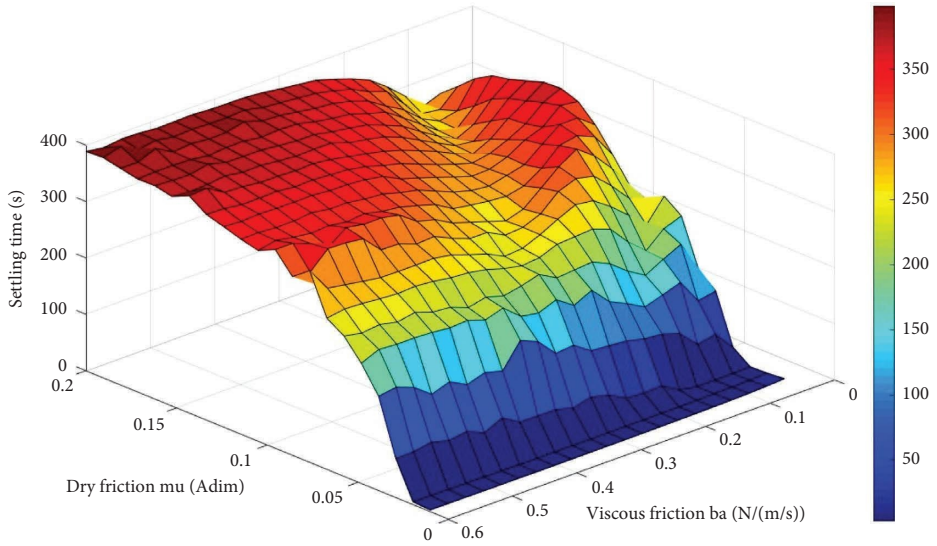

Figure 10: Settling time value for different values of μ and b_a. Second model with TMD.

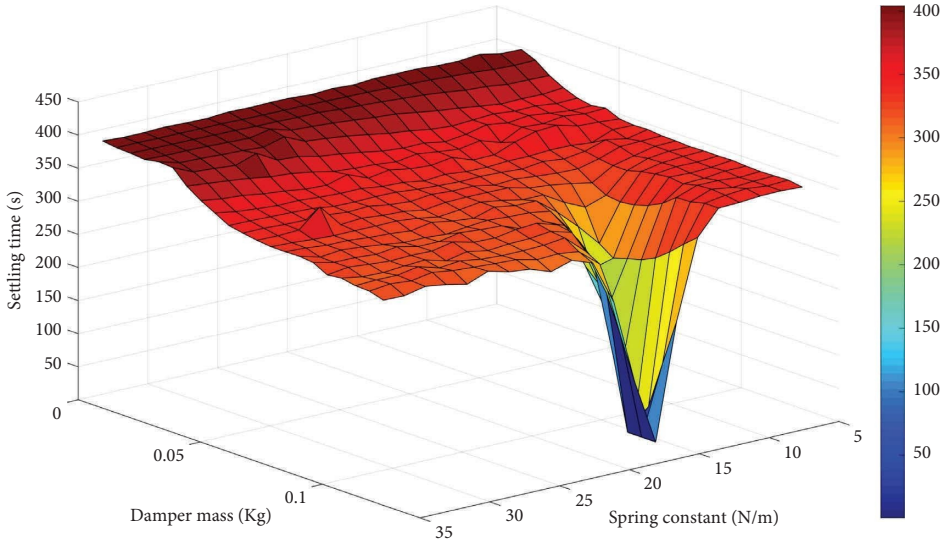

Figure 11: Settling time value for different values of m_a and k_a. Second model with TMD.

4.2. Vibration with TMD. The vibration with TMD refers to the end effector-free vibration in the z_f direction using a TMD. This model is represented by equations (25) and (26). The parameters dry friction μ and viscous friction b_a are generally not optimized due to the difficulty of setting and maintaining an exact value. The damper is usually designed so that the damping coefficients are within a convenient range of values. To know this convenient range, simulations were run in which b_a and μ were varied, keeping the other parameters constant ($m_a = 0.067$ and $k_a = 12$). The results are shown in Figure 10. It is observed that to achieve the objective of keeping the settling time low, it is convenient to maintain low values of both viscous friction and dry friction, but dry friction has a greater influence.

The optima values to know in this second model are the damper mass m_a and the spring constant in damper k_a. These are related to the mass and spring of the AMS. To achieve this, the second model was used, and these parameters were varied

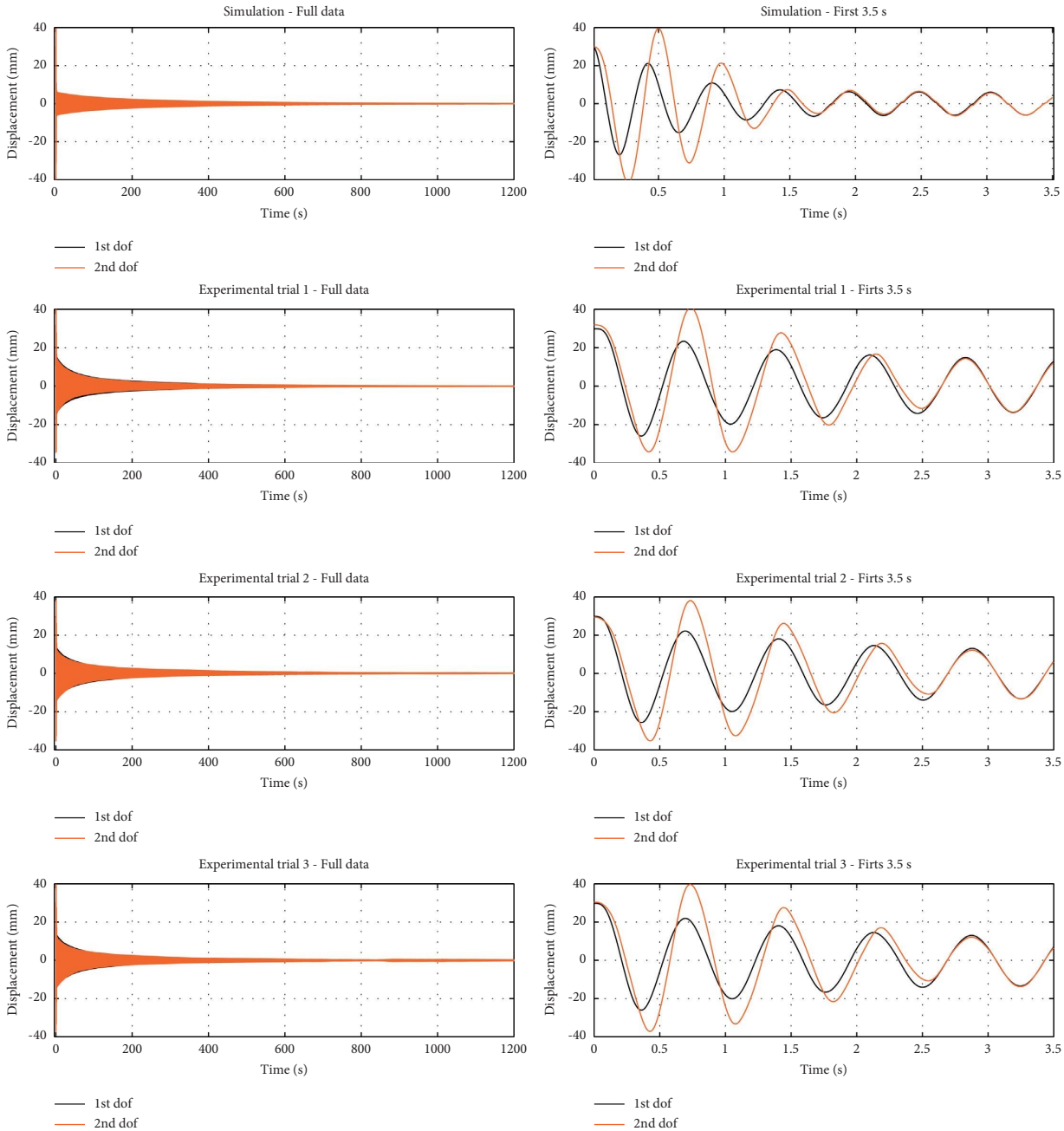

Figure 12: Real and simulated data of time response with TMD. Second model with TMD.

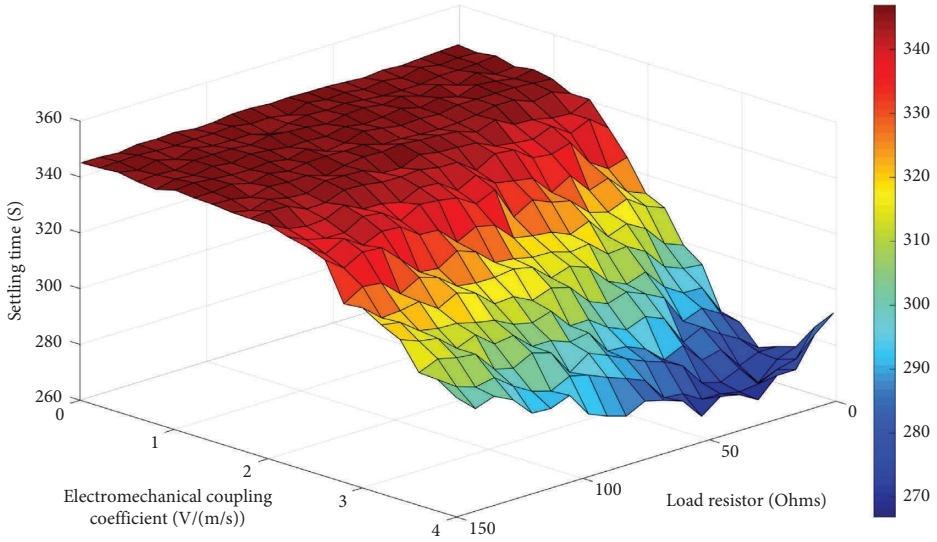

FIGURE 13: Settling time value for different values of C_{em} and R_l. Third model with ETMD.

to form a three-dimensional curve where the response variable is the settling time. It is shown in the Figure 11. The friction parameters used were $\mu = 0.1$ and $b_a = 0.4$.

Figure 12 shows the time response vibration of the first and second degrees of freedom with the implementation of a TMD. The graphs are shown in a 4 by 2 arrangement, in the first row the simulated data from the second model are shown, in the subsequent rows the three experimental tests are shown. In the first column the complete data is shown and in the second column a detail of the first 3.5 s is shown. In all cases the initial conditions of the free vibrations were positions of 30 mm for the two degrees of freedom. This shows the effect of TMD on vibration with respect to time. It also highlights the similarities between analytical and experimental data.

4.3. Vibration with ETMD. The vibration with ETMD refers to the end effector-free vibration in the z_f direction with the use of an ETMD. This third model is represented by equations number 31 and 32. The variables to optimize in this third model are the electromechanical coupling coefficient C_{em} and the load resistor R_l. The values of the frictions are $b_a = 0.105$, $m_a = 0.105$ and the rest of the parameters are kept according to the values previously established. A surface with simulated results is shown in Figure 13.

Figure 14 shows the time response vibration of the first and second degrees of freedom with the implementation of an ETMD. The graphs are shown in a 4 by 2 arrangement, in the first row the analytical data results of the simulation of the mathematical model are shown, in the subsequent rows the three experimental tests are shown. The first column contains the complete data and the second column has the details of the first 3.5 s. In all cases the initial conditions of the free vibration were positions of 30 mm for the two degrees of freedom. This shows the effect of ETMD on vibration with respect to time. It also highlights the similarities between analytical and experimental data.

4.4. Comparison of the Three Cases. The summary of the settling times for each of the three cases, both simulated and real are shown in Table 2 and Figure 15. The decrease in vibration settling time of the first degree of freedom can be appreciated before the implementation of the TMD and ETMD damping strategies. In Figure 5, the vertical axis represents the settlement time in seconds, the three models are presented on the horizontal axis. From right to left, the first set of data is the vibration settling times of the first degree of freedom without a damper, first model. The second set of data shows the settling time of the first degree of freedom using a TMD, second model. The last group of data, located to the right of the graph, represents the vibration setting times of the first degree of freedom before the implementation of a ETMD, third model. The graph clearly shows the decrease in the settling time of the first degree of freedom when using AMS and AEMS.

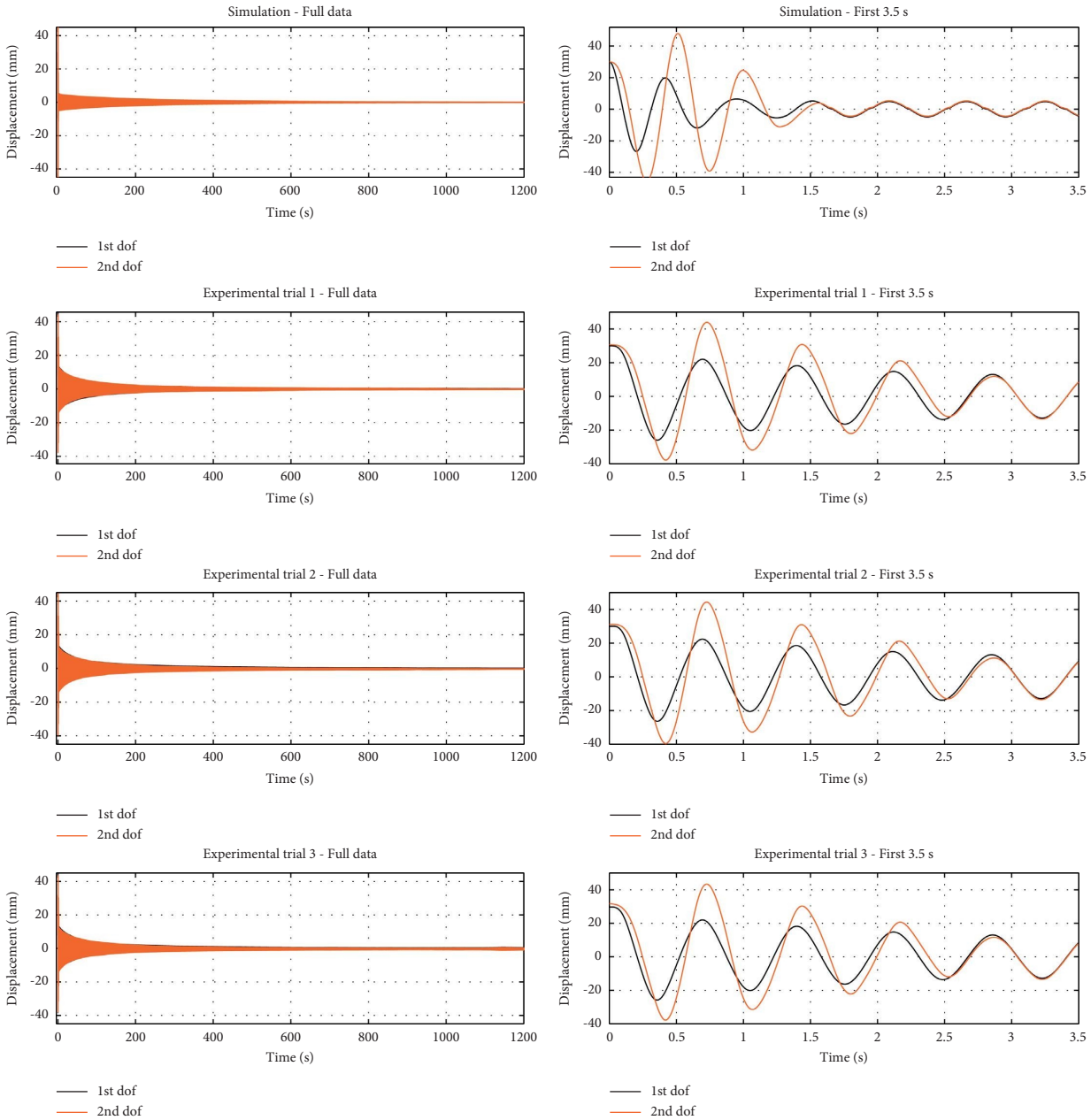

Figure 14: Real and simulated data of time response with ETMD. Third model with ETMD.

Table 2: Settling times.

	Free vibration (s)	AMS (s)	AEMS (s)
Simulated	369.16	324.57	292.15
Test 1	390.88	333.96	289.64
Test 2	375.62	328.47	289.24
Test 3	365.75	305.84	287.29

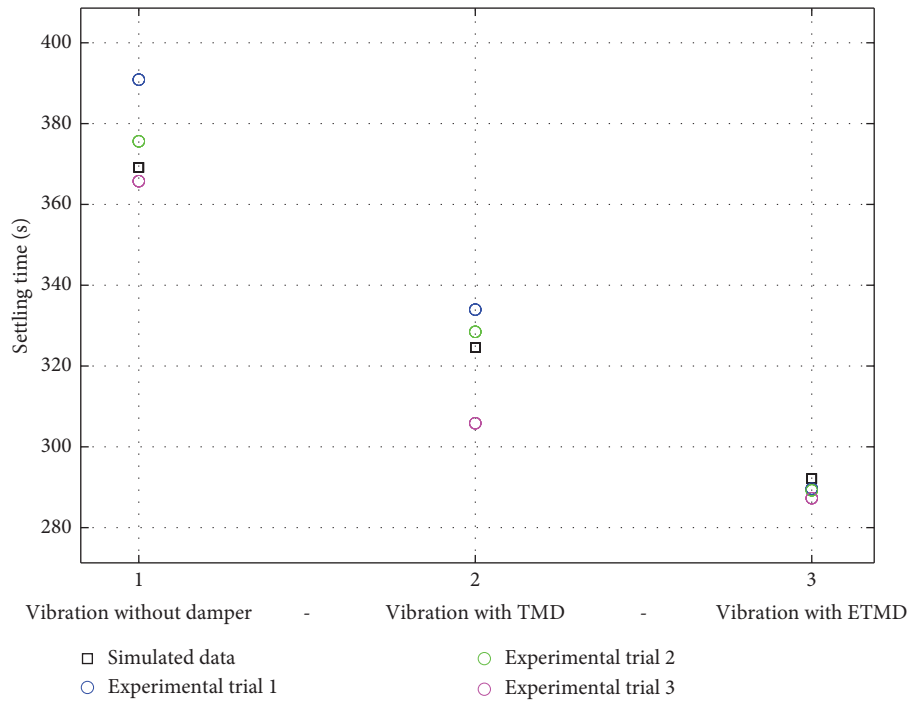

Figure 15: Comparison between settling times in cases without damper, with AMS and with AEMS.

5. Conclusions

In this research, the effectiveness of TMD and ETMD in reducing the settling time of free vibrations in planar CDPRs was evaluated. A numerical and experimental validation approach was proposed. Three mathematical models were assembled that represent three configurations of the dynamic system. A test bench was designed and built. It consisted of an eight-wire oscillatory dynamic system. In this, experimental tests of vibration without damper, vibration with TMD, and vibration with ETMD were performed.

From the results, it was found that the out-of-plane vibrations in planar CDPRs have peculiar characteristics compared to other conventional linear oscillatory systems. It was known from experimental observations, that this oscillation has long settling times and large vibrational amplitudes compared to the vibration of its other five degrees of freedom. With the fully defined mathematical model, not only the oscillatory behaviour can be predicted but the parameters can also be manipulated to obtain the desired behaviour or convenient settling time according to the context.

With the implementation of the TMD, an effective reduction of the settling time vibration in the first degree of freedom was achieved. The reduction of the settling time occurs during the first seconds of the oscillation, in which the two degrees of freedom oscillate at different positions and speeds. After these seconds, both degrees of freedom behave as one. This is due to the dry friction component present between the first and second degrees of freedom. The reduction in settling time depends on the selected parameters. It is theoretically possible to obtain reductions of 95%.

With the implementation of the ETMD, a reduction in settling time depends strongly on the frictions. This is because the implementation of an AEMS has the effect of increasing the coefficient of viscous friction in an equivalent AMS system; therefore, it could reduce or increase the settling time. That is, if the AMS parameter setting is at a point where an increase in viscous friction would imply a decrease in the settling time, then AEMS will reduce the settling time, as it works by increasing the coefficient of viscous friction between the first and second degrees of freedom. The opposite case can also be presented.

The practical utility of this study is to decrease the settling time for out-of-plane vibrations in CDPRs with planar configurations. Knowledge about the influence of dampers parameters on settling time has been generated and the selection of a successful combination of parameters will depend on the context of the application. In some cases, it will be necessary to keep the relationship between the mass of the end effector and the mass of the structure at a low value. In this case, it will be necessary to manipulate the other available parameters. In other cases, the mass of the damper may not have much space to move, requiring increasing the rigidity of the damper spring to limit its movement. In these cases, the mass parameters of the shock absorber or friction could be manipulated. In any of the cases mentioned and others that may arise, the use of the mathematical models developed will be useful to define the appropriate values of the parameters. The selling point of this method compared to others is that it does not require increasing the tension on the cables, greatly increasing the end-effector mass, or implementing an active solution. These mentioned solutions require external power.

As future work, it is recommended to explore the new applications of the geometrically nonlinear oscillations composed by cable planar configurations, as there is a great potential for investigations there. Also, it is suggested to extend the research to forced vibrations.

Data Availability

The datasets generated during and analysed during the current study are available from the corresponding author upon reasonable request.

Conflicts of Interest

The authors declare that there are no conflicts of interest.

Acknowledgments

The authors disclosed receipt of the following financial support for the research of this article: This work was supported by the Mexican government through the CONACYT scholarship system (grant no. 449316) and the support of the PAPIIT UNAM (grant no. IT102122) with the name "Diseño y construcción de un dispositivo y banco de pruebas para evaluar el daño efectuado a patrimonio cultural e histórico de México durante su desmontaje, preparación, traslado, montaje y exhibición."

References

[1] T. Higuchi, A. Ming, and J. Jiang-yu, "Application of multi-dimensional wire cranes in construction," in *Proceedings of the 5th ISARC*, Tokio, Japan, 1988.

[2] N. G. Dagalakis, J. S. Albus, B.-L. Wang, J. Unger, and J. D. Lee, "Stiffness study of a parallel link robot crane for shipbuilding applications," *Journal of Offshore Mechanics and Arctic Engineering*, vol. 111, no. 3, pp. 183–193, 1989.

[3] V. Mattioni, E. Idà, and M. Carricato, "Force-distribution sensitivity to cable-tension errors in overconstrained cable-driven parallel robots," *Mechanism and Machine Theory*, vol. 175, Article ID 104940, 2022.

[4] S. Kawamura, W. Choe, and S. T. S. Pandian, "Development of an ultrahigh speed robot FALCON using wire drive system," in *Proceedings of the 1995 IEEE International Conference on Robotics and Automation*, Nagoya, Japan, May 1995.

[5] S. Kawamura, H. Kino, and C. Won, "High-speed manipulation by using parallel wire-driven robots," *Robotica*, vol. 18, no. 1, pp. 13–21, 2000.

[6] O. Ma, X. Diao, Dynamics analysis of a cable-driven parallel manipulator for hardware-in-the-loop dynamic simulation," in *Proceedings of the 2005 IEEE/ASME International Conference on Advanced Intelligent Mechatronics*, Monterey, CA, USA, July 2005.

[7] X. Weber, L. Cuvillon, and J. Gangloff, "Active vibration canceling of a cable-driven parallel robot using reaction wheels," in *Proceedings of the de IEEE/RSJ International Conference on Intelligent Robots and Systems*, Chicago, IL, USA, September 2014.

[8] B. Zi, B. Duan, J. Du, and H. Bao, "Dynamic modeling and active control of a cable-suspended parallel robot," *Mechatronics*, vol. 18, no. 1, pp. 1–12, 2008.

[9] M. Rushton and A. Khajepour, "Optimal actuator placement for vibration control of a planar cable-driven robotic manipulator," in *Proceedings of the de American Control Conference (ACC)*, Boston, NJ, USA, July 2016.

[10] R. D. Rijk, M. Rushton, and A. Khajepour, "Out-of-plane vibration control of a planar cable-driven parallel robot using a multi-Axis reaction system," *Transactions on Mechatronics*, vol. 23, no. 4, pp. 1684–1692, 2018.

[11] M. A. Khosravi and H. D. Taghirad, "Dynamic modeling and control of parallel robots with elastic cables: singular perturbation approach," *IEEE Transactions on Robotics*, vol. 30, no. 3, pp. 694–704, 2014.

[12] V. Mattioni, E. Ida', and M. Carricato, "Design of a planar cable-driven parallel robot for non-contact tasks," *Applied Sciences*, vol. 11, no. 20, p. 9491, 2021.

[13] R. Villaverde, "Reduction seismic response with heavily-damped vibration absorbers," *Earthquake Engineering & Structural Dynamics*, vol. 13, no. 1, pp. 33–42, 1985.

[14] F. Sadek, B. Mohraz, A. W. Taylor, and R. M. Chung, "A method of estimating the parameters of tuned mass dampers for seismic applications," *Earthquake Engineering & Structural Dynamics*, vol. 26, no. 6, pp. 617–635, 1997.

[15] G. Bekdas and S. M. Nigdeli, "Estimating optimum parameters of tuned mass dampers using harmony search," *Engineering Structures*, vol. 33, no. 9, pp. 2716–2723, 2011.

[16] A. Z. G. Diego, C. R. R. Alejandro, P. C. L. Ma, J. Eden, and D. Oetomo, "On the use of tuned mass dampers for reducing the nonlinear vibrations of planar parallel cable robots," *International Journal of Mechanical Engineering and Robotics Research*, vol. 8, no. 3, pp. 406–412, 2019.

[17] D. A. Zamora-Garcia, L. M. Acosta-Carrion, M. X. Zepeda-Fuentes, M. P. Corona-Lira, and A. C. Ramirez-Reivich, "Numerical and experimental investigation of a cable-based nonlinear tuned mass damper to reduce free and forced vibrations," *International Journal of Mechanical Engineering and Robotics Research*, vol. 9, no. 10, pp. 1371–1378, 2020.

[18] A. J. Fleming and S. O. R. Moheimani, "Inertial vibration control using a shunted electromagnetic transducer," *IEEE*, vol. 11, no. 1, pp. 84–92, 2006.

[19] X. Tang and L. Zuo, "Simultaneous energy harvesting and vibration control of structures with tuned mass dampers," *Journal of Intelligent Material Systems and Structures*, vol. 23, no. 18, pp. 2117–2127, 2012.

[20] L. Zuo and W. Cui, "Dual-functional energy-harvesting and vibration control: electromagnetic resonant shunt series tuned mass dampers," *Journal of Vibration and Acoustics*, vol. 135, no. 5, Article ID 510181, 2013.

[21] Y. B. Bedoustani, H. D. Taghirad, and M. M. Aref, "Dynamics analysis of a redundant parallel manipulator driven by elastic cables," in *Proceedings of the 2008 10th International Conference on Control, Automation, Robotics and Vision*, Hanoi, Vietnam, December 2008.

[22] D. A. Zamora-Garcia, L. M. Acosta-Carrion, M. P. Corona-Lira, and A. C. Ramirez-Reivich, "Experimental determination of axial viscoelasticity of braided steel cables through the design of a special purpose machine," in *Proceedings of the de International Mechanical Engineering*

Congress and Exposition IMECE, Salt Lake City, Utah, USA, November 2019.

[23] B. Tang and M. Brennan, "A comparison of two nonlinear damping mechanisms in a vibration isolator," *Journal of Sound and Vibration*, vol. 332, no. 3, pp. 510–520, 2013.

[24] S. H. Nitzan, M. L. Valentina Zega, C. H. Ahn, A. Corigliano, and T. W. K. D. A. Horsley, "Self-induced parametric amplification arising from nonlinear elastic coupling in gyroscope," *Scientific Reports*, vol. 5, pp. 1–6, Article ID 9036, 2015.

[25] J. C. Carranza, M. J. Brennan, and B. Tang, "Sources and propagation of nonlinearity in a vibration isolator with geometrically nonlinear damping," *Journal of Vibration and Acoustics*, vol. 138, no. 2, 2016.